

Mechanochemical reaction in graphane under uniaxial tension

N.A.Popova and E.F.Sheka

Peoples' Friendship University of the Russian Federation, 117198 Moscow, Russia

sheka@icp.ac.ru

Abstract. The quantum-mechanochemical-reaction-coordinate simulations have been performed to investigate the mechanical properties of hydrogen functionalized graphene. The simulations disclosed atomically matched peculiarities that accompany the deformation-failure-rupture process occurred in the body. A comparative study of the deformation peculiarities related to equi-carbon-core (5,5) nanographene and nanographene sheets exhibited a high stiffness of both bodies that is provided by the related hexagon units, namely benzenoid and cyclohexanoid, respectively. The two units are characterized by anisotropy in the microscopic behavior under elongation along mechanochemical internal coordinates when the later are oriented either along (*zg*) or normally (*ach*) to the C-C bonds chain. The unit feature in combination with different configuration of their packing with respect to the body C-C bond chains forms the ground for the structure-sensitive mechanical behavior that is different for *zg* and *ach* deformation modes. Hydrogenation of graphene drastically influences behavior and numerical characteristics of the body making tricotage-like pattern of the graphene failure less pronounced and inverting it from the *zg* to *ach* mode as well as providing less mechanical resistance of graphane it total.

1. Introduction

Among chemically modified graphenes, graphane takes a peculiar position due to optimistic expectations of its production in valuable quantities, on one hand, and intense studies of its electronic, vibrational, and mechanical properties, on the other. Among the studies, dominate extended theoretical calculations while experimental investigations have been restricted until now by a single work [1]. What makes graphane so attractive? Sure, this firstly concerns electronic properties of a new 2D solid provided by opening bad gap. Secondly, graphane is expected to possess unique mechanical strength comparable with that one of graphene, which is supported by numerous calculations [2-7]. The latter, related to the main topic of the current paper, were mainly concentrated on the evaluation of elastic parameters of the 2D graphane crystal within the framework of an isotropic continuum elastic shell model and only Ref. 2 and 7 raised the issue on spatial dependence of mechanical behavior of graphane.

Calculations [3-7] were performed by using DFT unit-cell approximation with periodic boundary conditions (PBC). All of them are mutually consistent concerning elastic parameters obtained but none of them discloses how the graphane deformation proceeds and what mechanism of the graphane body fracture takes place. In contrast, a general view on the graphane fracture behavior has been presented by molecular dynamics calculations of a large graphane sheet [2]. The computations have disclosed a crack origin in the sheet body, the crack gradual growth, and a final sheet fracture. The situation is similar to that one occurred by the middle of 2009 concerning deformation of graphene [8]. A large number of computations, preferably in DFT supercell PBC, provided elastic parameters of graphene when the mechanical behavior of the graphene nanostructures remained unknown. Molecular dynamic calculations applied to long armchair-edged graphene nanoribbon [8] have thrown light on a peculiarity of the ribbon deformation disclosing the formation of one-atom chain in due course of uniaxial tension,

which was confirmed experimentally [9, 10]. This peculiar behavior has been highlighted and given in detail later from the viewpoint of mechanochemical reaction that lays the foundation of the deformation-failure-rupture process occurred in nanographenes [11, 12]. The quantum-mechanochemical-reaction-coordinate (QMRC) approach used in the study has disclosed atomically matched peculiarities of the mechanical behavior, highlighted the origin of the mechanical anisotropy of graphene, and made allowance for tracing a deformation-stimulated change in the chemical reactivity of both nanographene body and its individual atoms. And once again, the molecular dynamics study has shown that the fracture of not already graphene but graphane occurs in a peculiar manner pointing that more detail quantum chemistry insight is necessary.

In this paper, we present a comprehensive study of the mechanical properties of hydrogen functionalized graphene using QMRC approach simulations. We have found that hydrogenation has significant influence on the mechanical properties. Our simulations reveal that the tensile strength, fracture strain, and Young's modulus are sensitive to the functionalization. Basing on a detailed analysis of the deformation features, we attribute these significant changes in mechanical properties to the substitution of the benzenoid units of graphene by cyclohexanoids of graphane. Our simulations reveal that the elastic part of the deformation is vibration-involving so that the ratio of Young's moduli of graphene and graphane well correlated with the ratio of squared frequencies of the species valence C-C vibrations and/or internal phonons.

2. Methodology and computational details

2.1. Graphane isomerism

As mentioned in Introduction, graphane is mainly the subject of computational studies. Through over the computations, it is considered as a product of the graphene hydrogenation that preserves a honeycomb composition of the carbon core. However, in contrast to unified benzenoid structure of graphene units, the honeycomb cell of the 2D hydrogenated graphene crystal should be attributed to a particular cyclohexanoid unit, whose rich conformer biography, in contrast to benzenoid, has to be taken into account. This circumstance raises a definite question: which conformational honeycomb structure of hydrogenated graphene should be assigned as graphane? Is it a strictly determined monoconformer (which one in the case?) structure or is it just any arbitrary hydrogenated graphene that is implied in a predominant majority of computational studies? Historically, graphane $(CH)_n$ was introduced as a regular package of chairlike cyclohexanoid units [13]. This assignment was supported in [1] attributing the product of both-side hydrogenated membrane fixed by perimeter to this very structure. A clear crystalline-like image of X ray diffraction pattern convincingly justified the suggestion. In spite of no evidence of regular 2D packing of other cyclohexanoid conformers has been so far obtained, computational studies do not exclude 2D $(CH)_n$ crystals consisting of boat- [13], table- [14], zigzag- and/or armchair- [15], and stirruplike [16] cyclohexanoids thus making graphane's isomerism quite rich. Energetic preference of a chairlike conformer is naturally a strong argument for it to be the main representative of the graphane family. However, since different conformers of cyclohexane coexist and since their relative contribution depends on kinetic conditions of the reaction due to which the species is produced, a coexistence of different graphane isomers cannot be excluded as well. For the first time, the graphane isomerism has been considered in due course of computational stepwise hydrogenation of graphene [17]. The study has shown that when 1) all the edge carbon atoms located over perimeter of the pristine graphene sheet are fixed thus simulating a fixed membrane and 2) the sheet is accessible for hydrogen atoms from both side, a regularly packed chairlike cyclohexanoid's set presenting graphane $(CH)_n$ is obtained. At any other conditions, a non-regular packing of mixed cyclohexanoid conformers occurs, which causes a considerable distortion of a flat pristine

graphene sheet. Therefore, the chairlike graphane is not only energetically, but topologically the most preferable graphane isomorph. The finding is in a good consistence with the transformation of fixed graphene membrane, accessed to the atomic hydrogenation from both side, to graphane, which was observed experimentally [1]. As was shown therewith, no similar or any other regular structure was observed under one-side hydrogenation. Therefore, there are strong reasons, both computational and experimental, to limit oneself with chairlike conformer of the honeycomb cell of the 2D hydrogenated graphene crystal when speaking about graphane.

2.2. Graphane as object for uniaxial tension

Nanographane sheet studied in the current paper is shown in Fig.1. The species was obtained in due course of stepwise hydrogenation of (5,5) nanographene [17], a few steps of which is presented in the figure. The same (5,5) nanographene was previously subjected to uniaxial tensile deformation [11, 12], which provides a perfect basis for a comparative study of the mechanical behavior of the pristine and chemically modified bodies.

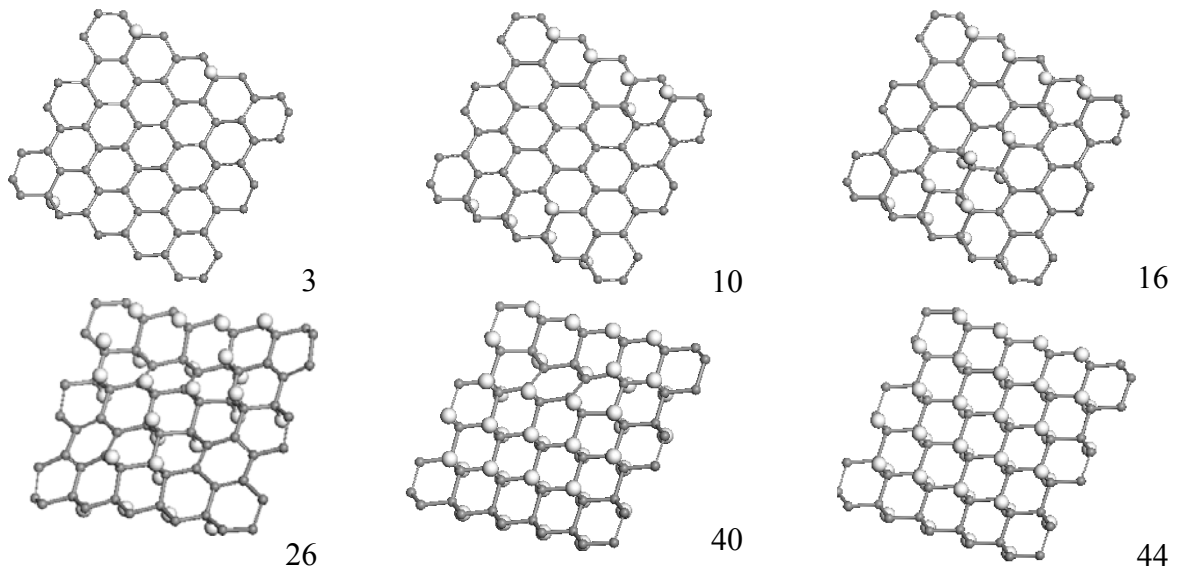


Figure 1. Equilibrium structures related to the stepwise hydrogenation of (5,5) nanographene [17]. Big white balls present hydrogen atoms. Figures point step numbers. Framing hydrogen atoms are not shown for simplicity.

Specifying uniaxial tension as a particular deformation mode within the framework of QMRC approach [18], one has to introduce specific mechanochemical internal coordinates (MICs). Obviously, such coordinates can be introduced by different ways with respect to carbon atom's positions in the sheets. In what follows we have restricted ourselves by two possibilities of the MICs determination orienting them either along the C-C bonds or normally to the latter. Thus determined two sets of MICs, topologically identical for both nanographene and nanographane, are shown in Fig. 2. The two sets distinguish two deformational modes that correspond to tensile deformation applied to either zigzag or armchair edges of the sheets due to which they are nominated as *zg* and *ach* modes as was done previously in [11, 12]. The right ends of the MICs in Fig.2 are clamped (the corresponding carbon atoms are immobilized) while the left ends move in a stepwise manner with increment $\delta L = 0.1 \text{ \AA}$ at each step so that the current MIC length constitutes $L = L_0 + m\delta L$, where L_0 is the initial length of the MIC and m counts the number of the deformation steps. According to the QMRC concept, the MICs are excluded from

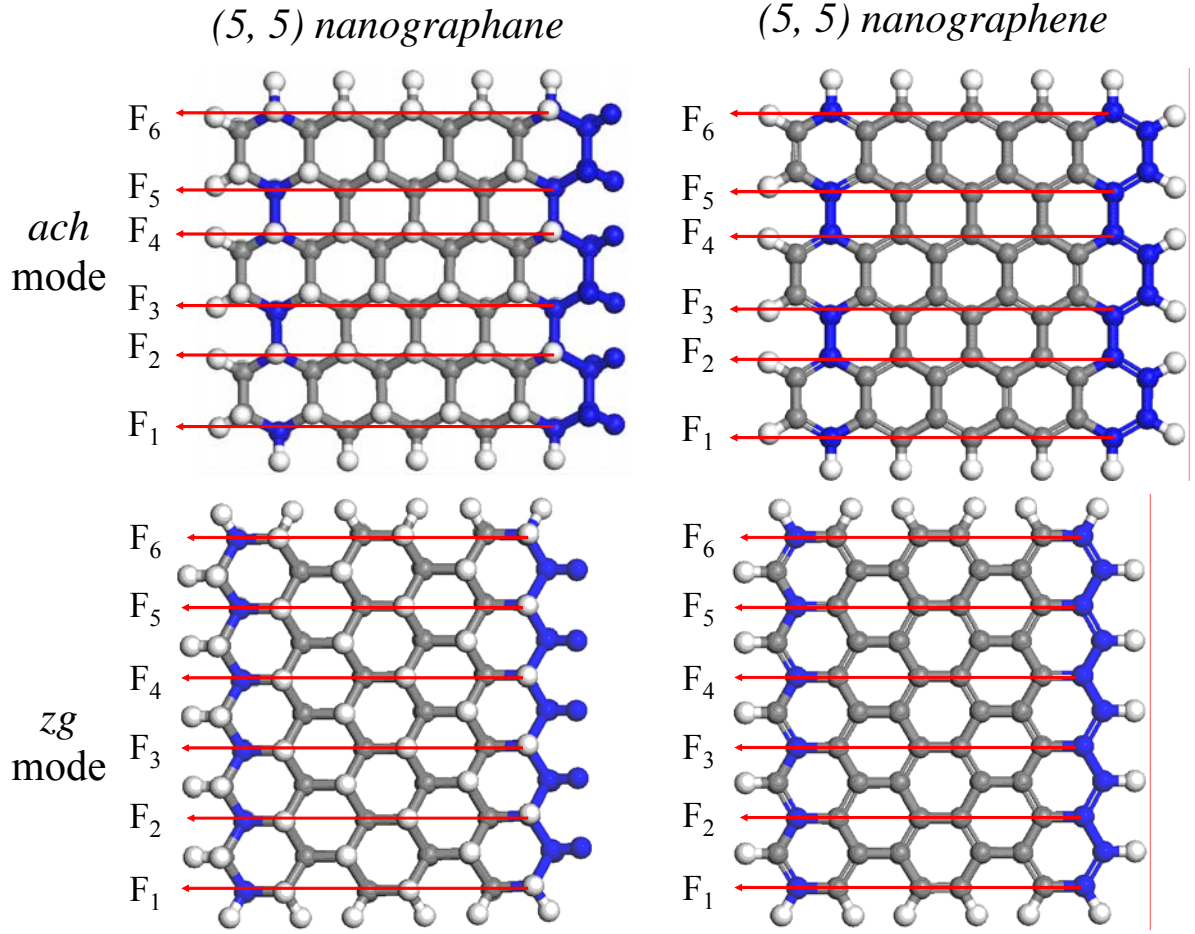


Figure 2. Configuration of six MICs related to two deformation modes of graphane and graphene (5,5) nanosheet. White and gray balls mark hydrogen and carbon atoms in equilibrium position. Edge carbon atoms are terminated by two and one hydrogen atoms for graphane and graphene, respectively. Atoms marked in blue are excluded from the optimization procedure. We use (n_a, n_z) nomenclature of rectangular nanographenes suggested in [19].

the optimisation procedure when seeking the minimum of the total energy. A *force of response* is determined as the residual gradient of the total energy along the selected MIC. These partial forces F_i are used afterwards for determining micro-macroscopic mechanical characteristics related to uniaxial tension, among which there are:

- Force of response F :
$$F = \sum_i^{MIC \text{ number}} F_i ; \quad (1)$$

- Stress σ :
$$\sigma = F / S = \left(\sum_i^{MIC \text{ number}} F_i \right) / S , \quad (2)$$

where S is the loading area determined as $S = DL_{0_z(a)}$ and where D is either the van der Waals thickness of the sp^3 -bending carbon-atom chain of 4.28\AA (graphane) or the van der Waals diameter of carbon atom of 3.34\AA (graphene) and $L_{0_z(a)}$ is the initial length of the MICs in the case of zg and ach modes, respectively;

- Young's modulus E :
$$E = \sigma / \varepsilon , \quad (3)$$

where both stress σ and strain ε are determined within the elastic region of deformation that starts at the MIC's length l_0 so that

$$\varepsilon = (L_i - l_0)/l_0 \quad (4)$$

in the general case [18]. The current length L_i is related to a particular deformation mode and within the mode is identical for all the MICs in the current experiment.

Implementation of the QMRC concept in the framework of DYQUAMECH software [20] that is based on the Hartree-Fock unrestricted version of the CLUSTER-Z1 codes exploiting advanced semiempirical QCh method (PM3 in the current study) [21]. The program retains all features of the unrestricted broken symmetry (UBS) approach, particularly important for odd electronic systems of graphene [22]. A completed computational cycle provides the following data.

Microscopic characteristics that include

- (i) the atomic structure of the loaded sheet body at any stage of the deformation including C-C bond scission and post-breaking relaxation;
- (ii) the strain energy

$$E_s(\varepsilon) = E_{tot}(\varepsilon) - E_{tot}(0) \quad (5)$$

where $E_{tot}(0)$ and $E_{tot}(\varepsilon)$ are the total energy of unloaded sample and sample subjected to ε strain, respectively;

- (iii) both partial and total (1) force of response;
- (iv) molecular and atomic chemical susceptibilities of the body expressed in terms of the total N_D and atomically partitioned N_{DA} numbers of effectively unpaired electrons [21], respectively.

The dependences of energy, force, stress and N_D on either elongation or strain exhibit mechanical behaviour of the object at all stages of the deformation considered at the atomic level [11, 12]. The latter presents changing in the chemical activity of the body in due course of deformation.

Micro-macroscopic characteristics involve stress-strain interrelation (2) that allow for introducing convenient elastic mechanic parameters similar to those of the elasticity theory.

3. Nanographene and/or nanographane under tensile deformation

3.1. *ach* Mode of the deformation

The identity of the carbon skeletons of both pristine graphene [11, 12] and graphane (5,5) nanosheets makes it possible to skip some details concerning the description of the sheet mechanical behavior presented in [11, 12] and to mainly concentrate on this behavior difference under hydrogenation. A sketch of the main characteristics related to the *ach* mode of the graphene tensile deformation and failure is shown in Fig.3a. As discussed in [11, 12], the sheet is uniformly stretched in due course of first 18 steps and breaking the C-C bonds occurs at the 19th step [23]. The sheet is divided in two fragments, one of which is a shortened (5,4) equilibrated nanographene while the other presents an alternative acetylene-and-carbene chain. The force-elongation dependence shows one-stage process of the sheet deformation and failure. The N_D -elongation exhibits a gradual increase in the sheet chemical activity up to the 19th step caused by a gradual elongation of C-C bonds, after which an abrupt grow of the chemical activity occurs at the 20th step caused by a simultaneous rupture of six C-C bonds. The achieved N_D value remains then constant and not dependent on the distance between two fragments of the

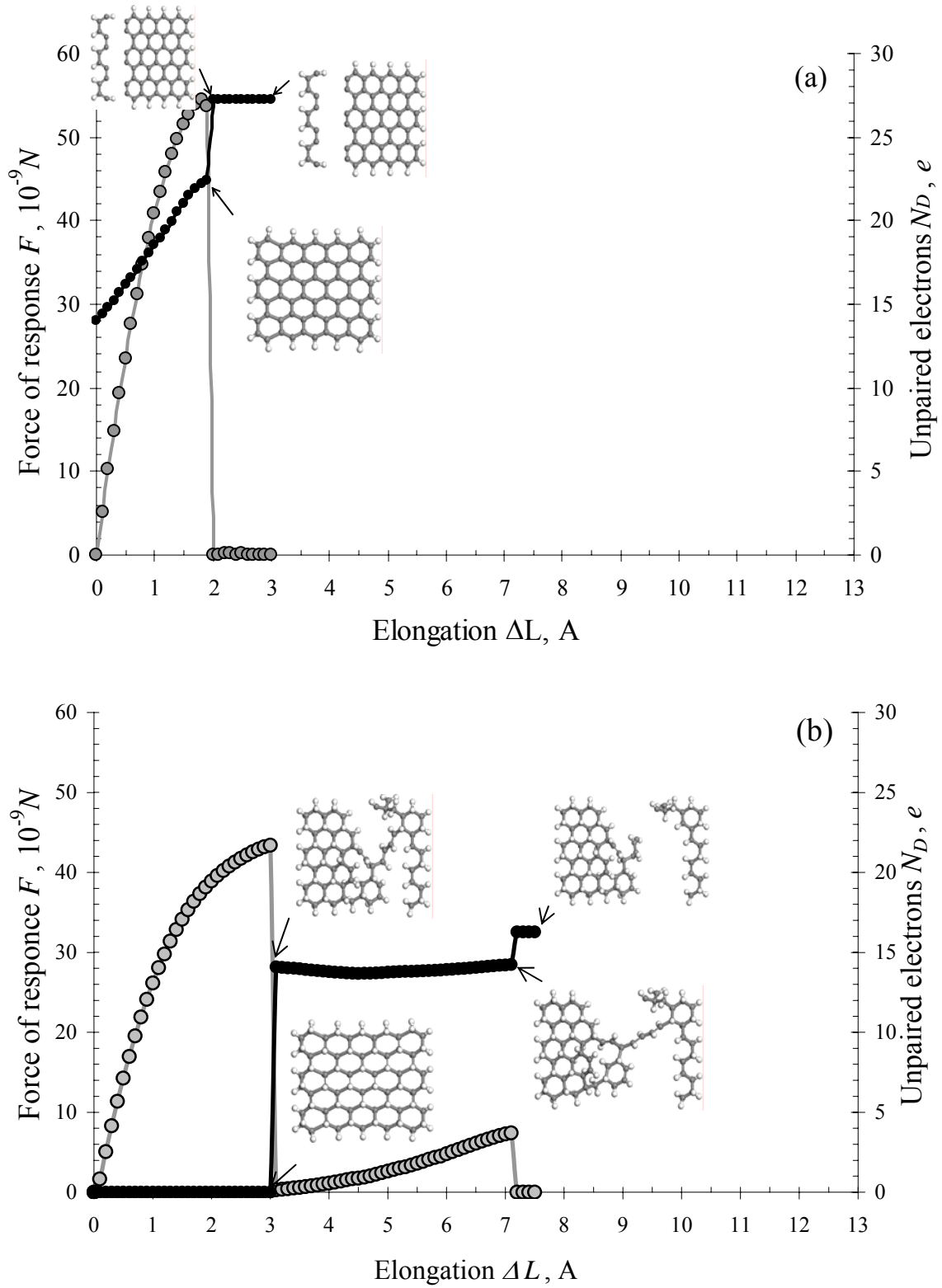


Figure 3. *ach* Deformation mode. Force-elongation (gray curve with dots, left Y-axis) and N_D -elongation (black curve with dots, right Y-axis) dependences and a selected sets of structures related to (5,5) nanographene (a) and nanographene (b) (see text). Arrows points the relation of the structures to the dots on the N_D -elongation curves.

broken nanographene. Structures presented in the figure are related to the 19th, 20th and 30th steps of the reaction.

As shown in Fig.3b, the *ach* deformation mode of graphane occurs quite differently. The force-elongation curve evidences a two-stage deformation process. During the first stage, the

nanosheet is firstly uniformly stretched similarly to graphene, but the stretching area is enlarged up to the 31st step. The stretching occurs without any C-C bond breaking since the number of effectively unpaired electrons N_D remains zero up to the 30th step. At the 31st step N_D abruptly grows up to 14 e , thus making the deformed sheet highly chemically active. The N_D growth is caused by the rupture of a number of C-C bonds and the formation of CH-unit linear chain that connects two fragments of the sheet as well as a small CH-unit cluster in the upper part of fragment 2. Further elongation causes a straightening of the chain, which takes additional 40 steps, after which the chain breaks and two separate fragments are formed. The chain breaking is accompanied by the second abrupt N_D grow and the achieved value remains unchanged when further elongation proceeds. Structures presented in the figure are related to the 30th, 31st, 70th, and 71st steps of the reaction. A detail comparison of the dynamic characteristics of the *ach* deformation mode of graphene and graphane will be done later. Here additionally to a qualitative difference in both nanosheets behavior, the attention should be drawn on 1.5 enlarging of the deformation area at the first step of deformation in graphane.

3.2. *zg* Mode of the deformation.

Figure 4a presents of a concise set of structure images of successive deformation steps revealing an exciting picture of a peculiar ‘tricotage’ failure of the pristine graphene body [11, 12]. On this language, each benzenoid unit presents a stitch and in the case of the *ach* mode shown in Fig.3a, the sheet rupture has both commenced and completed by the rupture of a single stitch row. In the case of the *zg* mode, the rupture of one stitch is ‘tugging at thread’ the other stitches that are replaced by still elongated one-atom chain of carbon atoms. This causes a saw-tooth pattern of both force-elongation and N_D -elongation dependences. In contrast to the multi-stage behavior of the pristine graphene, the *zg* mode of the graphane failure has commenced and completed within the first stage (see Fig.4b). Similarly to the situation occurred for the *ach* mode, the critical elongation is ~1.5 times bigger for the latter.

Looking at the data presented in Figs. 3 and 4, one can conclude that mechanical behavior of graphane differ from that one of graphene quite significantly. First, the hydrogenation effectively suppresses the tricotage-like pattern of the graphene deformation and failure. The hydrogen effect has been already shown in [11, 12] when passing from the deformation of the graphene nanosheet with bare edges to that one related to the sheet with hydrogen-terminated edges: this latter case is presented in Figs. 3 and 4. Sixteen-tooth force-elongation and N_D -elongation dependences of bare sheet are shorten to the eight-tooth pattern after termination of the edges by hydrogen atoms. However, once suppressed, the tricotage-like behavior has been still well exhibited in this case as seen in Fig.4a. A further hydrogenation, which concerns carbon atoms on basal plane of the sheet, smoothes the behavior further transferring a eight-tooth dependences in Fig.4a into two-tooth ones in Fig.3b thus shortening the scale of the deformation area from 12.1 to 7.2Å. Second, the multi-tooth pattern is characteristic for the *zg* mode of both bare-edge and hydrogen-terminated-edge of pristine graphene [11, 12] in contrast to one-stage deformation related to the *ach* mode thus showing the sheet to be more deformable along C-C bonds (see Fig.2). In contrast, a saw-tooth pattern is observed for the *ach* mode of the graphane deformation exhibiting higher deformability of the sheet along a C-C-C alkyl chain. The difference in the mechanical behavior related to *ach* and *zg* modes of graphene was attributed to the different configurations of the benzenoid stitch packing with respect to the body C-C bond chains. The same reason seems to lay the foundation of the anisotropy observed for the graphane sheet but addressed to the cyclohexanoid unit packing.

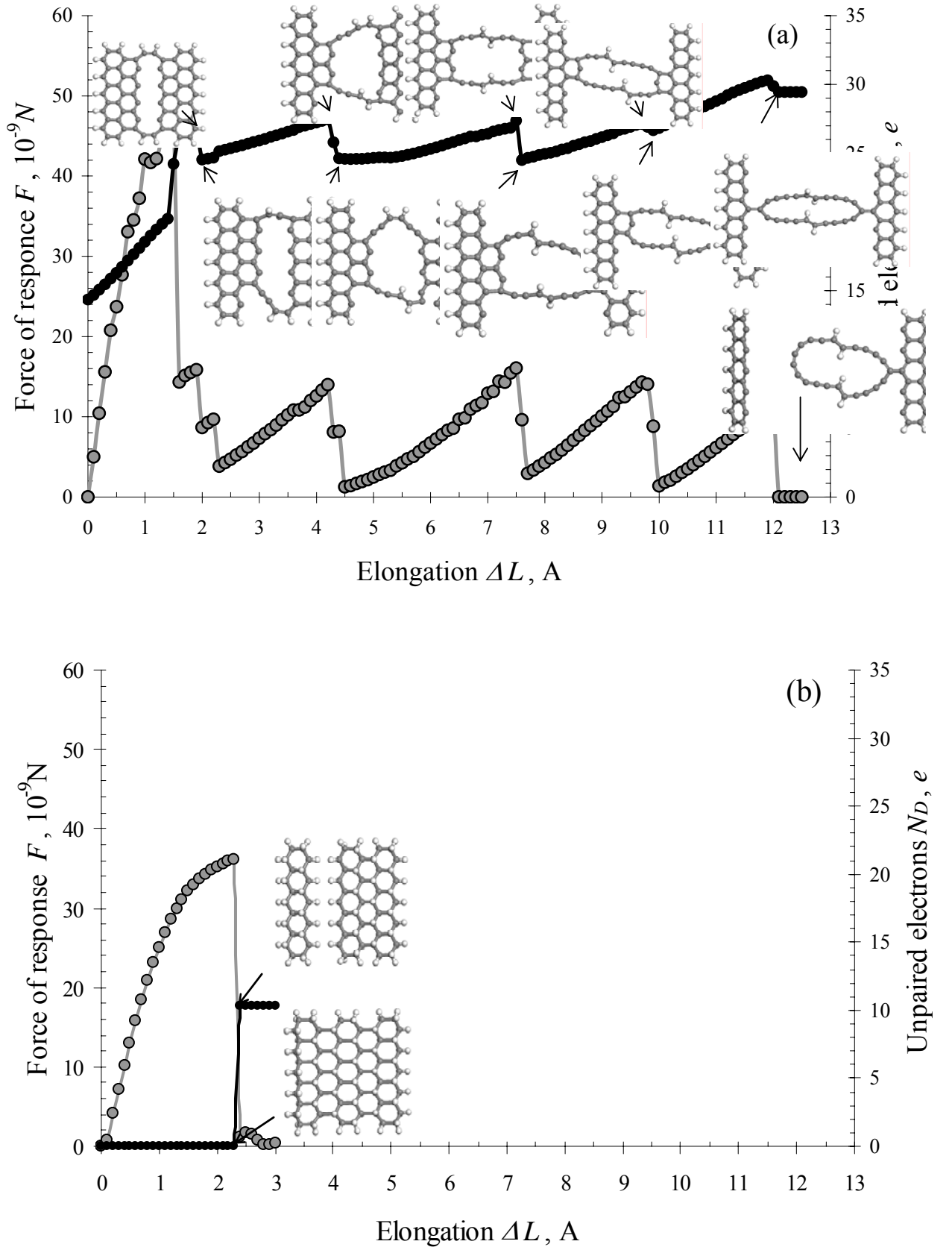


Figure 4. zg Deformation mode. Force-elongation (gray curve with dots, left Y-axis) and N_D -elongation (black curve with dots, right Y-axis) dependences and a selected sets of structures related to (5,5) nanographene (a) and nanographene (b) (see text). Arrows points the relation of the structures to the dots on the N_D -elongation curves.

4. Energetic characteristic of the graphane tensile deformation

The total energy of the graphane nanosheet subjected to tensile stress is presented in Fig.5a. At first glance, the plotting looks quite typical and seems to follow the concept of the elasticity theory in the region close to the initial MIC's length. More detail plotting of force of response in Fig.5b highlights some inconsistency with the elasticity approach in this region. As seen in the figure, the first two points on both curves do not subordinate the linear dependence and match the region named as rubbery high-elasticity state in the case of polymers where a similar situation has been met quite often [25, 18]. The elastic region is determined by a linear dependence of the force from the MIC elongation. Approximating the intersection of the linear dependence with the abscissa, the straight lines indicate reference MIC lengths, l_0 , which correspond to the start of the linear dependence, depicting the beginning of the elastic deformation. The l_0 values thus determined is used later when defining strain energy $E_s(\varepsilon)$ according to (5), whose dependence on strain ε expressed by (4) is presented in Fig. 5c, as well as stress-strain values in the region are plotted in Fig. 6. The plotting can be used to determine Young's moduli for the considered deformation modes.

Figure 6a well highlights the difference in mechanical behavior of *zg* and *ach* deformation modes of graphane. Leaving aside the two-tooth pattern of the stress-strain dependence for the *ach* mode, one can concentrate on the first stages of the deformation in both cases that evidently govern quantitative values of the deformation parameters. As seen in the figure, both modes are practically non-distinguishable up to 12% strain after which the failure process proceeds much quicker for the *zg* mode and accomplishes at the 23% strain while the failure according to the *ach* mode continues up to 30% strain. The critical values of force of response F_{cr} , stress σ_{cr} , and strain ε_{cr} are presented in Table 1.

Table 1. Mechanical parameters of graphene and graphane

Species	Mode	ε (at σ_{cr})	F_{cr} , $N \cdot 10^{-9}$	σ_{cr} , $N/m^2 \cdot 10^9$	$E_{\sigma, \varepsilon}$, TPa
benzene	<i>ach</i>	0,29	19,62	120,47	0,76
	<i>zg</i>	0,22	19,18	97,13	0,99
cyclohexane	<i>ach</i>	0,44	15,69	93,76	0,4
	<i>zg</i>	0,36	14,99	74,57	0,74
(5, 5) nanographene	<i>ach</i>	0,18	54,56	119,85	1,09
	<i>zg</i>	0,14	47,99	106,66	1,15
(5, 5) nanographane	<i>ach</i>	0,3	43,41	74,37	0.61_{σ} (0.54 _{ε})
	<i>zg</i>	0,23	36,09	63,24	0.57_{σ} (0.52 _{ε})

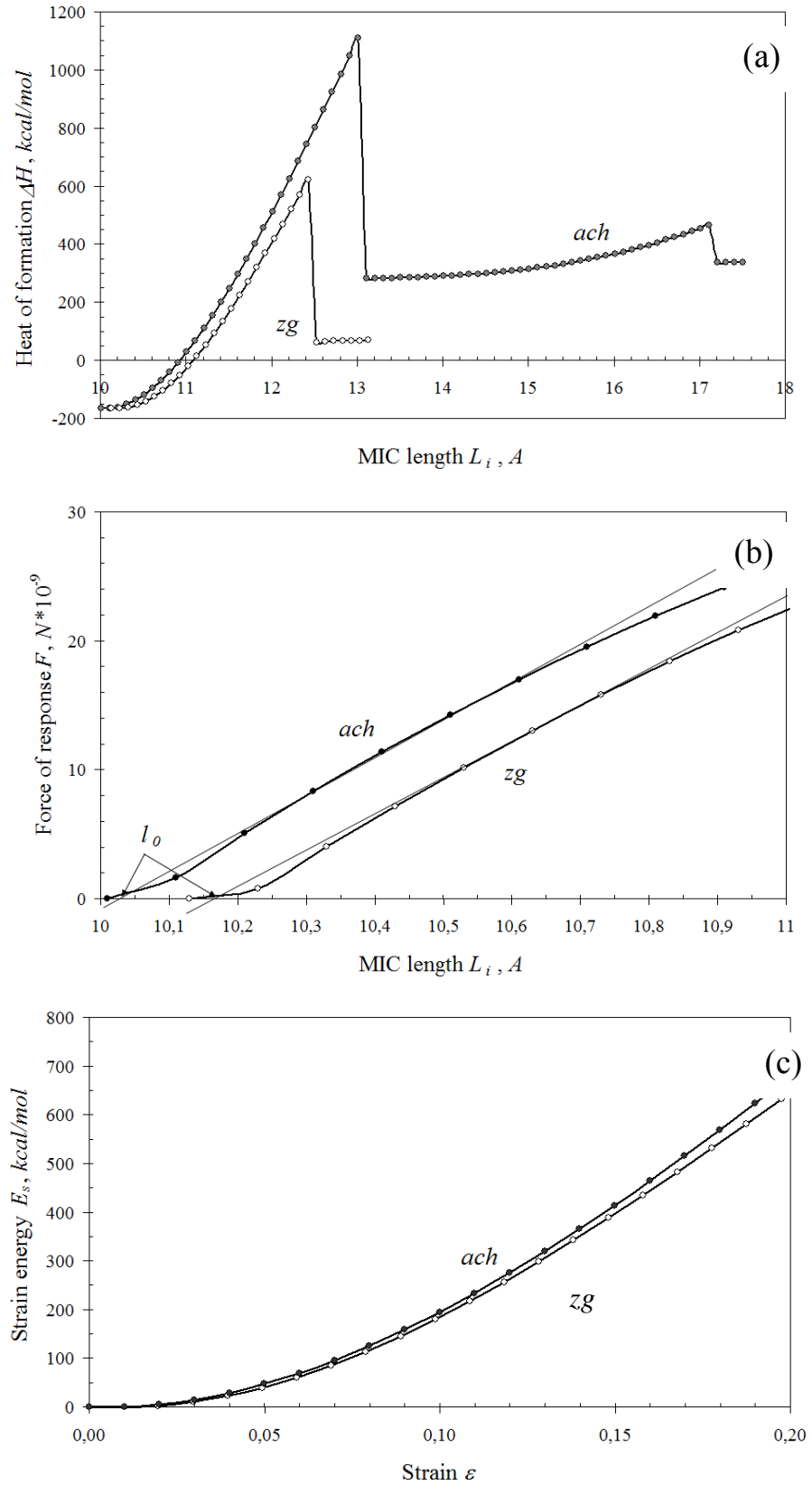


Figure 5. Dependence of total energy (a) and force of response (b) on MIC's length as well as strain energy on strain (c) of (5,5) nanographane. Filled and empty circles match *ach* and *zg* deformation modes, respectively.

Once non-distinguishable by eyes, the stress-strain regularities of the two modes related to the first stage of the deformation are nevertheless different as shown in Figs. 6b and 6c.

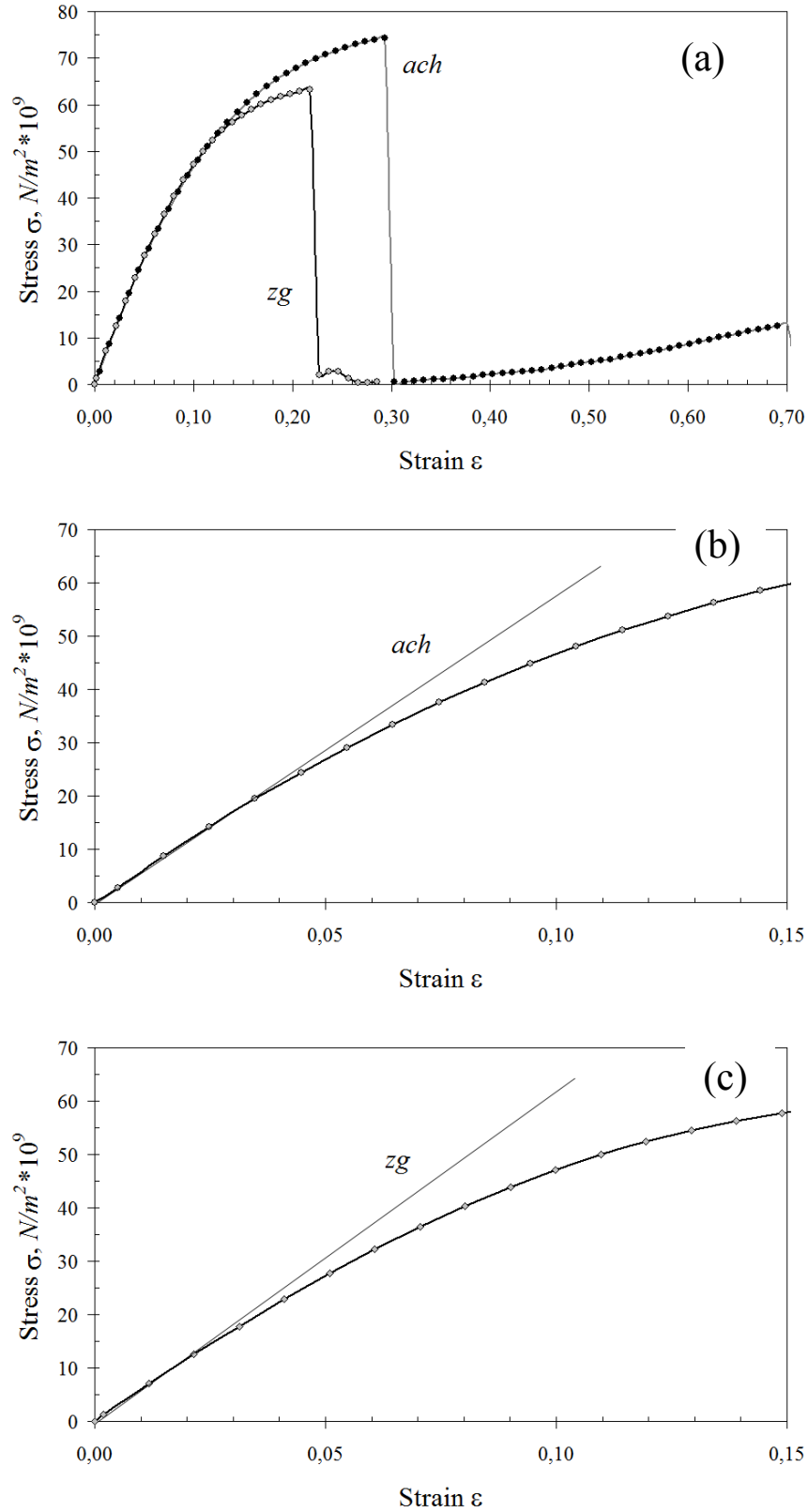


Figure 6. Stress-strain relationship for (5,5) nanographane subjected to tensile deformation (a) and that one at the first deformation steps related to *ach* (b) and *zg* (c) modes.

Firstly, the difference concerns the size of the region attributed to the elastic behavior of the plottings. As seen in the figures, the *ach* deformation is elastic up to the strain reaching 4%

while in the zg mode the elastic region is shorter and is commenced on 2% strain. However, practically about half of the region in both cases is not elastic but corresponds to the rubbery high-elasticity state as shown in Fig.5b. Therefore, the graphene deformation is mainly non-elastic, once rubbery high-elastic at the very beginning and plastic after reaching 4% (ach) and 2% (zg) strain. The values of Young's moduli E_σ attributed to the elastic parts of stress-strain plottings in Figs. 6b and 6c are given in Table 1.

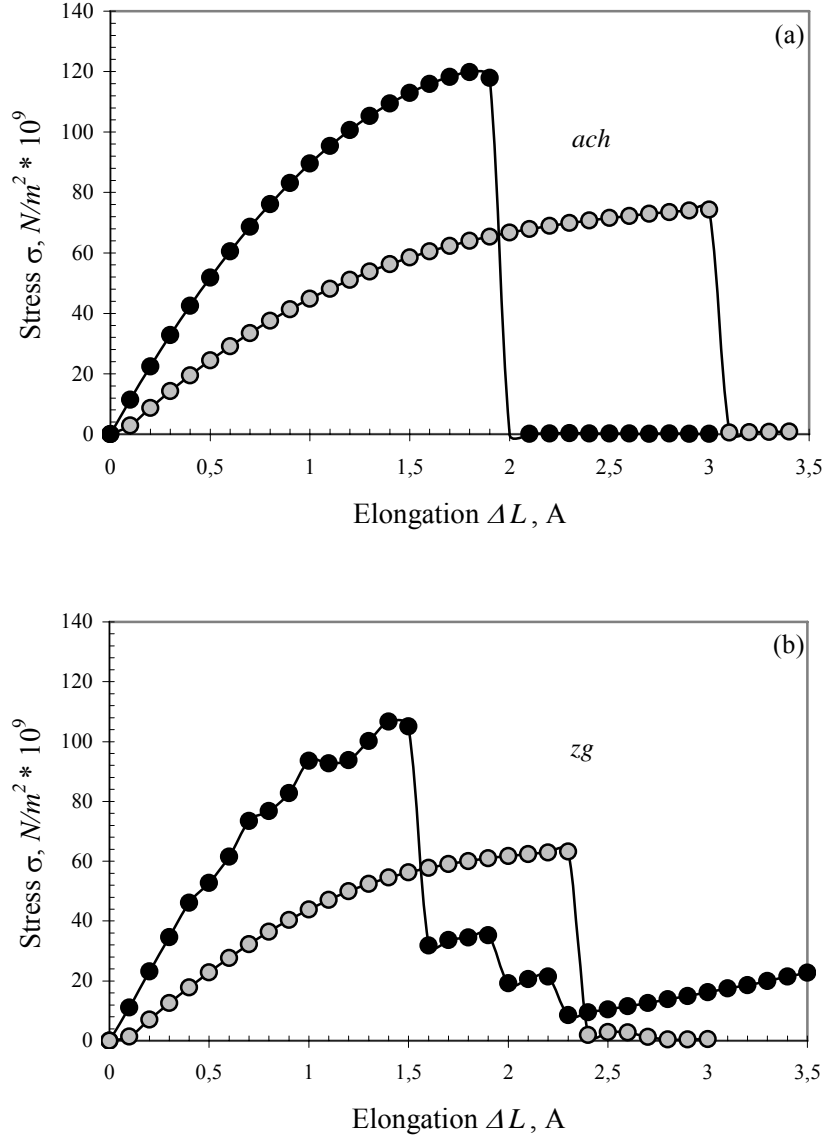


Figure 7. Stress-strain relationship for graphene (black dots) and graphene (gray dots) (5,5) nanosheet subjected to tensile deformation related to ach (b) and zg (c) modes at the first stage of deformation.

As well known, another way to determine Young's module is addressed to the strain energy (5) that in the elastic approach can be presented as [25]

$$E_s(\varepsilon) = 1/2 v_0 E_e \varepsilon^2, \quad (6)$$

where v_0 is the volume involved in the deformation and E_e is the related Young modulus. Applying the approach to the initial part of E_s curves presented in Fig.5c it has been confirmed that the elastic approach fits the curves at the same regions of strains as determined for the stresses. Obtained E_e values are well consistent with the previously determined E_σ , as seen from Table 1.

To conclude the discussion of peculiarities of mechanic characteristics of graphane, a comparative view on the mechanical behavior of graphene and graphane is presented in Fig.7. The presentation is limited by the first stage of the graphane deformation. The figure exhibits quite clearly

- The existence of the rubbery high-elastic state at the beginning of the deformation in graphane while a similar state in the graphene deformation is absent so that the deformation of the latter in this region is elastic and the origin of the elastic behavior l_0 coincides with the initial MIC's length $L_{0_z(a)}$;
- Much less elasticity of graphane if one applies the elastic approach to the latter;
- The main part of the deformation of both bodies occurs in plastic regime;
- The graphane failure commences at much shorter elongation than that of graphene.

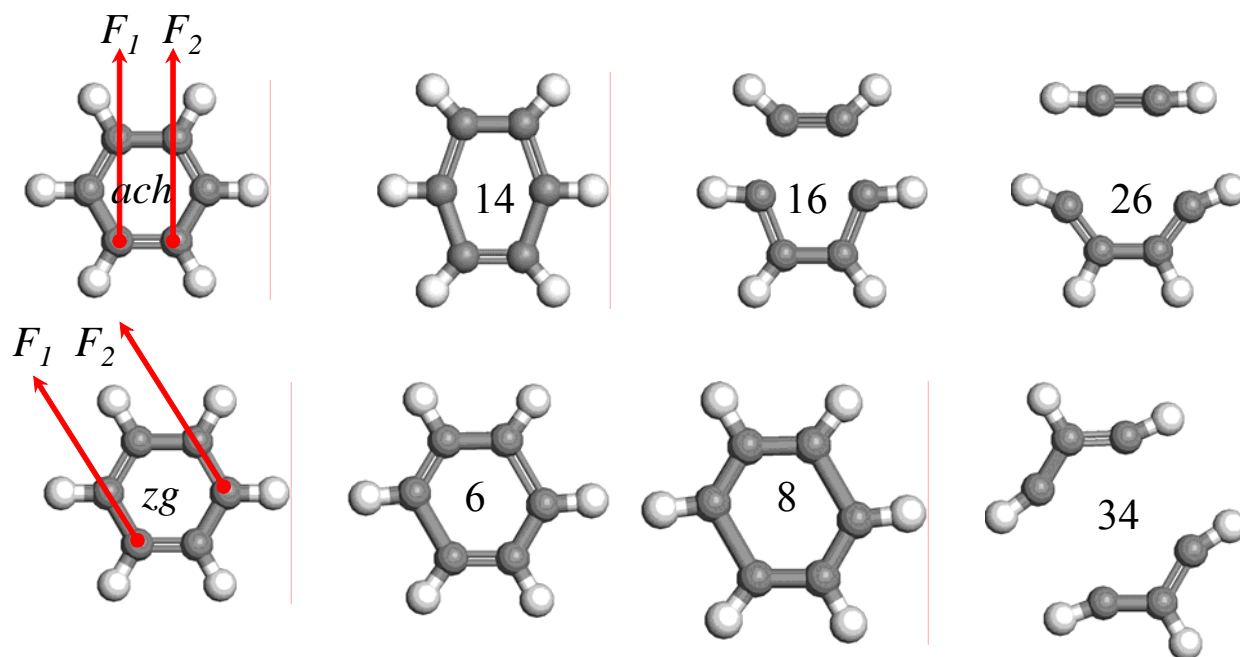
Alongside with the peculiarities discussed earlier that concern a suppress of the tricotage-like character of the deformation caused by hydrogenation, all the findings suggest a quite extended picture of the hydrogenation effect on mechanical properties of graphene. A native question arises what reasons are behind the observed features. Let us try to find answer addressing a molecular aspect of the discussed deformation process.

5. Molecular aspect of the graphene and/or graphane deformation

As was shown [11, 12], unique mechanic properties of graphene have originated from the mechanic resistance of its benzenoid units. Taking benzene (BZN) molecule as their molecular image, the QMRC approach has revealed a vividly seen mechanical anisotropy of the molecule which lays the foundation of the difference in the *ach*- and *zg*-mode's behavior of graphene. Table 1 lists the main mechanical parameters of the molecule that are well consistent with those related to the graphene body thus demonstrating the origin of the body's properties. In this view it is natural to draw attention to the mechanical properties of a molecule that might simulate the cyclohexanoid unit of graphane. Obviously, cyclohexane (CHXN) in its chairlike conformation should be the appropriate model. Figure 8 presents a set of structures of the benzene and cyclohexane molecules subjected to uniaxial tensile deformation described by two pairs of MICs that can be associated with the *ach* and *zg* modes discussed in the previous sections. Deformation proceeds as a stepwise elongation of both MICs at each deformation mode with a constant increment of 0.05Å per a step. Details of the computational procedure are given in [11, 12] for benzene molecule. As seen in the figure, deformation of both molecules at both deformation modes looks structurally quite similar as it might be taking into account the difference in chemical structures.

A comparative insight on the quantitative characteristics of the mechanical behavior of both molecules is summarized in Fig. 9. Stress-strain curves accumulate the mechanical behavior while N_D -strain curves exhibit changes in the chemical reactivity of the molecules in due course of the deformation. As seen in the figure, stress-strain curves show that sharp mechanic anisotropy of BZN is significantly smoothed for CHXN. The latter is evidently less elastic than BZN and is broken at less stress but at bigger strain in both modes. Changing in the chemical reactivity of the two molecules is evidently different since due to sp^2 character of the electron system of BZN, lifting N_D value over zero is observed already before the C-C bonds rupture, the latter adds additional increasing of the value at $\varepsilon > 0.4$. In contrast, N_D value for sp^3 hybridized

Tensile deformation of benzene



Tensile deformation of cyclohexane

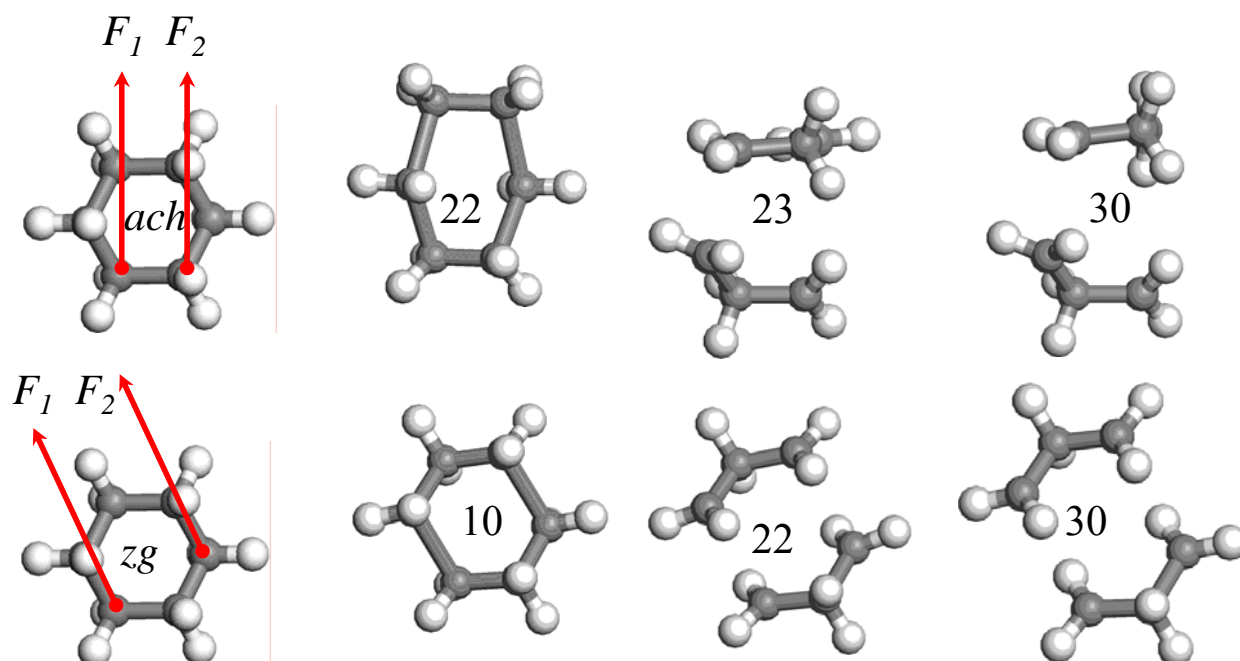


Figure 8. Equilibrium structures related to the stepwise tensile deformation of benzene and cyclohexane. The configuration of MICs related to *ach* and *zg* modes are shown in the left panels. Figures point step numbers.

CHXN retains zero until the C-C bonds rupture occurs at 23rd and 22nd steps of the *ach* and *zg* modes, respectively, when an abrupt N_D growth up to $\sim 4 e$ occurs. It should be noted that if the C-C bonds rupture in CHXN at *ach* mode is accompanied by the immediate N_D growth, in the case of *zg* mode the ND growth is somewhat postponed and occurs in 12 steps later until the formed fragments take the form of step 23 shown in Fig.8. The preceding 12 steps correspond to overstretched C-C bonds such as in the form of step 22 in Fig.8.

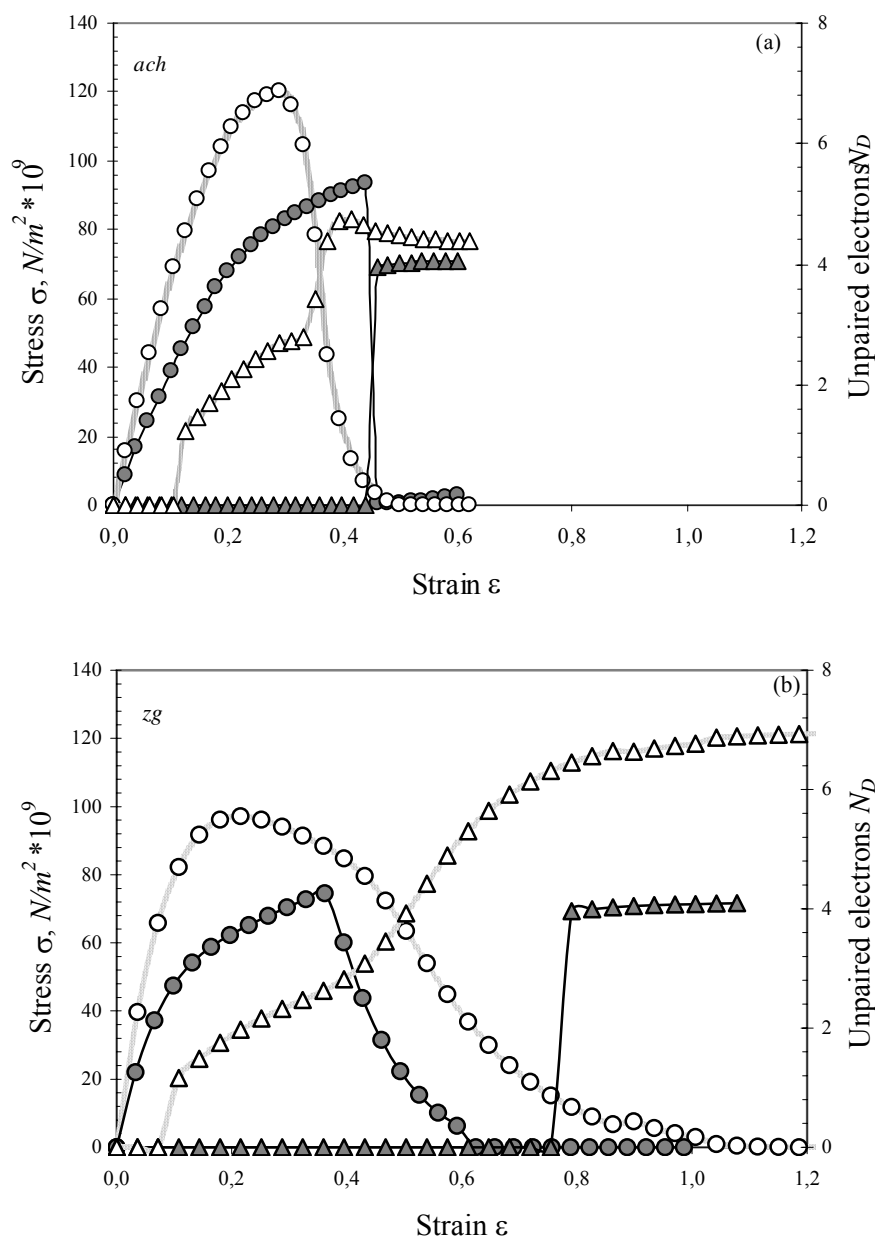


Figure 9. Stress-strain (circles, left Y-axis) and N_D -strain (triangles, right Y-axis) dependences related to (5,5) nanographene (empty) and nanographane (filled) at *ach* (a) and *zg* (b) deformation modes.

Mechanical characteristics of both molecules are presented in Table 1 alongside with those related to (5,5) nanographene and nanographane discussed in the previous sections. As clearly seen from the table, there is a close resemblance of the data related to the molecules and the condensed bodies. The very molecular characteristics explain why the graphane elasticity is lower, why the critical strains are bigger but critical stresses are smaller. Taking together these characteristics provide the lowering of Young's modulus of graphane in both deformation modes. Obviously, a complete coincidence of the molecular and condensed body data should not be expected since packing of both benzenoid and cyclohexanoid units must remarkably contribute into the mechanical behavior. The packing, which is anisotropic in regards C-C bond chains, seems to be responsible for the difference in the topology of the failure during the *ach* and *zg* modes. But, the asymmetry of the final products at the *ach* deformation of CHXN seems to be quite suitable for the creation of CH-unit chain when adjacent cyclohexanoid units are cracked.

6. Mechanical deformation and dynamic properties

Since every mechanical deformation is thought to be vibration-involving [25], there might be a tight connection between the mechanical behavior of the object and its vibrational and/or phonon spectrum. As shown for polymers [25], the elastic part of the behavior, which is provided by stretching of chemical bonds, is obviously connected with the relevant valence vibrations. The occurrence of the rubbery highly-elasticity state is usually attributed to a high conformational ability of polymers that is provided by low-frequency torsional and deformational vibrations [18]. In view of this concept, elastic parameters such as Young's modulus and stiffness must be proportional to force constants, or squared frequency, of the relevant harmonic vibrations.

In the current case, the deformation of both BZN and CHXN molecules and graphene/graphane bodies are determined by the rupture of C-C bonds. Frequency of the characteristic C-C valence vibrations of BZN constitutes $\nu_{C-C}^{BZN} = 1599 \text{ cm}^{-1}$ [26]. Taking ν_{C-C}^{BZN} as the reference, it is possible to determine the relevant frequency of CHXN ν_{C-C}^{CHXN} that has to provide the lowering of its Young's moduli using a relation

$$\nu_{C-C}^{CHXN} = \eta \nu_{C-C}^{BZN}, \quad (7)$$

where

$$\eta = \sqrt{(E_{\sigma}^{CHXN} / E_{\sigma}^{BZN})} \quad (8)$$

is the square root of the ratio of Young's moduli obtained for the molecule from the stress-strain curves. The obtained ν_{C-C}^{CHXN} values are given in Table 2. As seen from the table, those are in good consistence with two molecular frequencies of CHXN, which may evidence that different vibrations govern the elastic deformation of CHXN at two different deformation modes.

The phonon spectra of both graphene [28, 29] and graphane [30] are formed by broad bands whose attribution to C-C bond stretching is not so straightforward. In the case of graphene, a definite eigenvector phonon mode pointing to C-C stretching is related to the optical phonons at the Γ point of the Brillouin zone that produces a characteristic G-band at 1564 cm^{-1} observed in the species Raman spectrum [28]. Taking the frequency as the reference $\nu_{C-C}^{graphene}$, one can evaluate the corresponding graphane frequencies $\nu_{C-C}^{graphane}$ that have to provide the observed decreasing of Young's moduli presented in Table 2. The corresponding frequencies lie in the $1167\text{-}1071 \text{ cm}^{-1}$ region. The calculated graphane phonon spectrum [30] exhibit pure carbon-atom-involved and mixed carbon-atom-involved internal phonons in the region of $1000\text{-}1330 \text{ cm}^{-1}$ thus determining the region for expected η_{exd} value from 1.18 to 1.60, which is in a perfect consistence with the data presented in Table 2. Therefore, the lowering of Young's modulus of graphane with respect to graphene has a dynamic nature and is connected with a softening of C-C internal phonons when passing from sp^2 to sp^3 configuration. The softening is caused by the weakening of the corresponding C-C bonds, which was experimentally proven just recently [31].

Besides valence vibrations, hydrogenation of both benzene molecule and graphene provides appearance of low-frequency torsional and deformational vibrations [27, 30]. These vibrations do not influence much the deformation of an individual molecule but may affect significantly the behavior of condensed chains of the latter. It seems quite reasonable to suggest that the rubbery high-elastic state of the graphane deformation is just the appearance of a considerable softening of this low-frequency part of the phonon spectrum of graphane [30] with respect to graphene.

Table 2. Young's moduli and stretching C-C vibrations

Species	Def. mode	E_σ	η	$\nu_{C-C}^{CHXN}, \text{cm}^{-1}$	$\nu_{C-C}, \text{cm}^{-1}$	η_{exd}
BZN	ach	0.76	1.38	1159	1599 [24]	1.49
	zg	0.99				
CHXN	ach	0.40	1.16	1378	1388 [26]	1.15
	zg	0.74				
$\nu_{C-C}^{graphane}, \text{cm}^{-1}$						
graphene	ach	1.09	1.34	1167	1564 [26]	1.18-1.60
	zg	1.15				
graphane	ach	0.61	1.46	1071	1330-1000 [27]	
	zg	0.57				

The dynamic origin of the Young modulus lowering forces us to draw attention on the elastic parameters of fluorographene (CF)_n [32] since the phonon spectrum of the latter has been calculated [30]. According to calculations, C-C internal phonons fill the region 1100-1330 cm⁻¹, due to which one can expect decreasing of the Young modulus for the fluoride from 2 to 1.4, which is similar to graphane. The first observations [32] show 3 times decreasing in regards to graphene. Once complicated by difficulties inherited in the fluorographene production and indentation technique, the data nevertheless are in a reasonable consistence with the prediction.

7. Conclusion

In summary, we have carried out systematic quantum-mechanochemical-reaction-coordinate simulations to study the mechanical properties of graphane. The latter implies the chairlike conformer of cyclohexanoid units of the honeycomb packing of carbon atoms. We have found that the mechanical behavior of graphane is anisotropic similarly to graphene so that tensile deformation along (zg mode) and normal (ach mode) C-C bonds chain occurs quite differently. Nevertheless, typical to graphene tricotage-like pattern of the body failure is considerably suppressed. Besides that, the spatial region of elastic regime is remarkably shortened and a rubbery high-elasticity state has been exhibited. The tensile strengths at fracture constitute 62% and 59% of graphene for ach and zg modes, respectively while the fracture strains increase therewith by 1.7 and 1.6 times. The Young's moduli of the two deformation modes of graphane decrease by 1.8 and 2 times. Our simulations show that the main part of the change occurs at a molecular level and is provided by the substitution of benzenoid units of graphene by cyclohexanoid ones of graphane. Additional contribution is connected with the difference of the units packing in the honeycomb bodies. A vibration-involving deformation concept has been successfully applied to explain the decrease of the Young moduli connecting the latter with softening C-C stretching vibrations in due course of the *sp*²-to-*sp*³ bonding transition. A justified prediction concerning elastic parameters of fluorographene has been made.

Acknowledgement

The authors are grateful to L.Kh.Shaymardanova for assistance with modeling related to benzene and cyclohexane molecules.

References

1. Elias, D. C.; Nair, R. R.; Mohiuddin, T. M. G.; Morozov, S. V.; Blake, P.; Halsall, M. P.; Ferrari, A. C.; Boukhvalov, D. W.; Katsnelson, M. I.; Geim, A. K.; Novoselov, K. S. *Science* **2009**, *323*, 610-613.
2. Pei, Q.X.; Zhang, Y.W.; Shenoy, V.B. *Carbon* **2010**, *48*, 898-904.
3. Munos, E.; Singh, A.K.; Ribas, M.A.; Penev, E.S.; Yakobson, B.I. *Diam. Rel. Mat.* **2010**, *19*, 368-373.
4. Topsakal, V.; Cahangirov, S.; Ciraci, S. *Appl. Phys. Lett.* **2010**, *96*, 091912.
5. Leenaerts, O.; Peelaers, H.; Hernandez-Nieves, A.D.; Partoens, B.; Peeters, F.M. *Phys. Rev. B* **2010**, *82*, 195436.
6. Cadelano, E.; Palla, P.L.; Giordano, S.; Colombo, L. *Phys. Rev. B* **2010**, *82*, 235414.
7. Scarpa, F.; Chowdhury, R.; Adhikari, S. *Phys. Lett. A* **2011**, *375*, 2071-2074.
8. Bu, H.; Chen, Y.; Zou, M.; Yi, H.; Bi, K.; Ni, Z. *Phys. Lett. A* **2009**, *373*, 3359-3362.
9. Jin, C.; Lan, H.; Peng, L.; Suenaga, K.; Iijima, S. *Phys. Rev. Lett.* **2009**, *102*, 205501.
10. Chuvilin, A.; Meyer, J.C.; Algara-Siller, G.; Kaiser, U. *New Jour. Phys.* **2009**, *11*, 083019.
11. Sheka, E.F.; Popova, N.A.; Popova, V.A.; Nikitina, E.A.; Shaymardanova, L.K. *J. Exp. Theor. Phys.* **2011**, *112*, 602-611.
12. Sheka, E.F.; Popova, N.A.; Popova, V.A.; Nikitina, E.A.; Shaymardanova, L.K. *J. Mol. Mod.* **2011**, *17*, 1121-1131.
13. Sofo, J. O.; Chaudhari, A. S.; Barber, G. D. *Phys. Rev. B* **2007**, *75*, 153401.
14. AlZahrana, A.Z.; Srivastava, G.P. *Appl. Surf. Sci.* **2010**, *256*, 5783-5788.
15. Leenaerts, O.; Peelaers, H.; Hernandez-Nieves, A. D.; Partoens, B.; Peeters, F. M. *Phys. Rev. B* **2010**, *82*, 195436 [6 pages].
16. Bhattacharya, A.; Bhattacharya, S.; Majumder, C.; Das, G. P. *phys. stat. sol. (RRL)* **2010**, *4*, 368-370.
17. Sheka, E.F.; Popova, N.A. *arXiv: 1102.0922 [cond-mat.mes-hall]* **2011**.
18. Nikitina, E.A.; Khavryutchenko, V.D.; Sheka, E.F.; Barthel, H.; Weis, J. *J. Phys. Chem. A* **1999**, *103*, 11355-11365.
19. Khavryutchenko, V. D.; Khavryutchenko, A. V., Jr. *DYQUAMECH*, Dynamical-Quantum Modelling in Mechanochemistry Software for Personal Computers; Institute of Surface Chemistry, National Academy of Science of Ukraine: Kiev, 1993.
20. V.A. Zayets, *CLUSTER-ZI*, Quantum-Chemical Software for Calculations in the *s,p*-Basis; Institute of Surface Chemistry, National Academy of Science of Ukraine: Kiev, 1990.
21. Sheka, E.F.; Chernozatonskii, L.A. *J. Exp. Theor. Phys.* **2010**, *110*, 121-132.
22. Gao, X.; Zhou, Z.; Zhao, Y.; Nagase, S.; Zhang, S.B.; Chen, Z. *J. Phys. Chem. A* **2008**, *112*, 12677.
23. C-C bond is considered broken when the interatomic distance exceeds 2.15 Å (see details in [24]).
24. Sheka, E.F.; submitted
25. Tashiro, K.; Kobayashi, M.; Tadacoro, H. *Polymer Journ.* **1992**, *24*, 899-916.
26. Gribov, L.A.; Dementjev, V.A.; Todorovskii, A.T. Interpretirovanye kolebatel'nykh spektry alkanov, alkenov i proizvodnykh benzola (Assigned vibrational spectra of alkyls, alkenes, and benzene derivatives). Nauka: Moskva, 1986.
27. Elyashberg, M.E.; Karasev, Yu. Z.; Dementjev, V.A.; Gribov, L.A. Interpretirovanye kolebatel'nykh spektry uglevodorodov – proizvodnykh cykloheksana i cyklopentana (Assigned vibrational spectra of cyclohexane and cyclopentane derivatives). Nauka: Moskva, 1988c.
28. Mohr, M.; Maultzsch, J.; Dobardžić, E.; Reich, S.; Milošević, I.; Damnjanović, M.; Bosak, A.; Krisch, M.; Thomsen, C. *Phys. Rev. B* **2007**, *76*, 035439.
29. Adamyan, V.; Zavalniuk, V. *J. Phys.: Condens. Matter* **2011**, *23*, 015402.

30. Peelaers, H.; Hern'andez-Nieves, A. D.; Leenaerts, O.; Partoens, B.; Peeters, F. M. *Appl. Phys. Lett.* **2011**, 98, 051914 - 051914-3.
31. Sun, C.Q.; Sun, Y.; Nie, Y. G.; Wang, Y.; Pan, J. S.; Ouyang, G.; Pan, L. K.; Sun, Z. *J. Phys. Chem. C* **2009**, 113, 16464–16467.
32. Nair, R.R.; Ren, W.; Jalil, R.; Riaz, I.; Kravets, V.G.; Britnell, L.; Blake, P.; Schedin, F.; Mayorov, A.S.; Yuan, S.; Katsnelson, M.I.; Cheng, H.-M.; Strupinski, W.; Bulusheva, L.G.; Okotrub, A.V.; Grigorieva, I.V.; Grigorenko, A.N.; Novoselov, K.N.; Geim, A.K. *Small* **2010**, 6, 2877–2884.